Single Chain Entanglement: A Monte Carlo Simulation of Dilute Solution Capillary Electrophoresis

M. E. Starkweather, M. Muthukumar,* and D. A. Hoagland

Department of Polymer Science and Engineering and Materials Research Science and Engineering Center (MRSEC), University of Massachusetts, Amherst, Massachusetts 01003

Received November 10, 1997; Revised Manuscript Received June 2, 1998

ABSTRACT: The configurational interactions of a single flexible polyelectrolyte probe chain driven at moderate electric field through a single neutral frozen host chain are investigated using the Monte Carlo simulation method. The simulated probe length varies from 25 to 200 Kuhn steps, while the host length remains fixed at 200 Kuhn steps; the probe's charge density and the medium's Debye−Hückel screening length constitute additional parameters. The simulations reveal a strong and chain length dependent entanglement coupling between probe and host, consistent with recent experiments demonstrating that polyelectrolytes can be electrophoretically separated by molecular weight in a dilute solution of neutral polymers. Additionally, charge density and Debye−Hückel screening length are shown to be important factors in the separation mechanism, affecting both the probability of coupling and the duration of resulting entanglements. The scaling exponent relating entanglement time to molecular weight lies between the values of 2 and 3, the respective limits for Rouse and reptation disentanglement dynamics.

1. Introduction

Interest in capillary electrophoresis for macroion separation has grown dramatically in the past decade, with the technique increasingly used to separate and sequence proteins, DNA restriction fragments, and other polyelectrolytes. Recently, much attention has focused on applications of capillary electrophoresis that employ a dilute neutral polymer solution in place of the traditional gel media.[1−4] The substitution allows a more complete realization of the speed, efficiency, and automation of the capillary geometry but also changes, in a profound way, the underlying molecular dynamics. Little is known about the new dynamics and how they relate to the corresponding dynamics in a gel. Yet, these dynamics must be understood to optimize existing separations and to extend the new capillary techniques to additional polymer systems.

The free solution electrophoretic mobility of double-stranded DNA and other uniformly charged polyelectrolytes displays little, if any, dependence on molecular weight.[5] To endow the needed dependence, electrophoretic separations are nearly always performed in the presence of a neutral support matrix, most often a semirigid cross-linked gel containing pores of molecular size. Although originally termed "anti-convective" agents, the role of the gel in the separation of polyions is considerably more active than this label suggests. The remarkable success of electrophoresis gels in fractionating polyelectrolytes by molecular weight has motivated theorists to develop separation models that focus on field-biased chain transport in rigid porous media; the models typically introduce variables such as gel concentration, probe/pore size ratio, and cross-link density. Despite significant and sustained effort,[6] the interaction between a migrating probe chain and the fixed host matrix remains incompletely understood. Recent reports suggest that neutral polymer solutions, prepared at concentrations below the entanglement threshold, comprise a suitable alternative media for electrophoretic separation of long chain molecules. Specifically, fast and efficient separations of DNA restriction fragments of up to 23 000 base pairs (bp) have been achieved with hydroxyethyl cellulose (HEC) solutions as low in concentration as 0.002 wt %.[3] Other un-cross-linked linear polymers have also been sucessfully exploited for DNA separation, including linear polyacrylamide,[7,8] methyl cellulose,[9] pullulan,[10] hydroxypropylcellulose,[11] glucomannan,[12] liquefied agarose,[13] and poly(ethylene oxide) (PEO).[14]

In a rigid gel matrix, the motions of a homologous series of probe chains can be roughly correlated with the ratio of average chain size to average pore size. Some investigators have justified similar descriptions for probe motion in entangled solutions by viewing these sluggish but fluidlike matrix materials as "virtual gels."[15] In a rigid gel, when the chain/pore size ratio is small, Ogston-type sieving appears to explain molecular weight dependent chain transport,[16,17] although the underpinnings of the original sieving theory by Ogston and others have been seriously questioned.[18,19] At the opposite extreme, when the chain/pore ratio is large, the reptation model describes transport with reasonable success,[20−24] especially with the model modified to account for field-induced chain orientation.[25−27] Finally for the intermediate case, when the relevant size ratio lies near unity, the entropic barriers model[28−31] suggests that a coupling of chain flexibility to medium inhomogeneity defines a regime of entropically activated transport. Unlike either sieving or reptation depictions, entropic barriers transport explicitly accounts for the spatial variation of configurational entropy for the confined probe chain. Plotting the electrophoretic mobility against the logarithim of molecular weight yields a curve with characteristics reflective of the three transport modes: the weak molecular weight dependence of sieving (obeying a stretched exponential function) yields to the stronger molecular weight dependence of entropic barriers transport (approximately exponential), which then yields to the more moderate molecular weight dependence of reptation or biased reptation (power law).

S0024-9297(97)01651-3 CCC: $15.00
Published on Web 07/23/1998

Extrapolating these gel concepts to the polymer solution environment remains a challenge, even accepting the virtual gel argument (the extent of entanglements in solutions being unknown). For example, are mobilities in the two settings equally sensitive to parameters characterizing the probe (average size, chain length and stiffness, charge density) and the host environment (ionic strength, matrix concentration, field strength)? Some trends are clearly unique to the solution experiment. For example, Barron et al. concluded that the resolving power of a host polymer depends on the polymer's chain length[2] and, along with Singhal and Xian,[32] that a low concentration of long host polymers provides better separation for a large probe than a high concentration of short host polymers where entanglements are absent. Visualization of DNA during electrophoresis in a dilute polymer solution suggests important roles for previously unobserved "oscillatory" and "waltzing" kinds of motions.[33,34]

Models for electrophoresis in dilute polymer solutions presumably must incorporate both the discrete and the transient nature of probe/host interactions. Periods of entanglement alternate with periods in which the probe chain moves by its molecular weight independent free solution mobility. Two simple theories have been proposed. Barron and co-workers[3] propose probe motion hindered by transient entanglement coupling with host molecules in which the probe size mobility discrimination occurs through the increased probability of probe−host entanglement as probe size increases. Hubert, Slater, and Viovy envisage a governing mechanism in which host polymers are dragged along by the migrating polyelectrolyte.[36] These mechanisms are fundamentally the same. They derive an expression for probe velocity that explicitly incorporates host size and concentration. Muthukumar[37] has also undertaken theoretical derivations in this area, deriving an explicit formula for polyelectrolyte electrophoretic mobility in semidilute neutral polymer sieving buffers. In calculating the electrophoretic mobility, friction of the probe polyelectrolyte against the matrix arising from the collisions and preaveraged hydrodynamic interactions are fully accounted for. Taking into account molecular weight, polymer concentration, solvent quality, and Debye−Hückel screening length, he has delineated three concentration dependent separation regimes.

Although polyelectrolyte electrophoresis has been the subject of numerous computer simulations, the literature contains few reports pertinent to experiments in a dilute, neutral polymer matrix.[38−44] Most relevent are the simulations of Sevick and Williams[45] and Nixon and Slater,[46] teams that have modeled the collisions of a polyelectrolyte chain with a single obstacle in two dimensions. Sevick and Williams examined collisions with a single pointlike obstacle, while Nixon and Slater investigated collisions with a circular obstacle placed in a narrow channel. Common to both simulations is a pully process of disentanglement. Neither team, however, made inquiry into the polymeric nature of the host obstacle or to the three-dimensional character of real entanglement dynamics.

We study the configurational interactions of a flexible probe during its motion through a fixed linear host, constructing both probe and host as three-dimensional, off-lattice, random walks. While the host is frozen and stationary, a Monte Carlo scheme allows for flexibility and preferential motion of the probe down a uniform electric potential gradient directed along the initial center-of-mass positions of probe and host. The field is of moderate strength, creating significant but incomplete orientation during entanglement coupling. The frequency and duration of entanglements are monitored as well as the dependence of these quantities on probe molecular weight, solvent quality, and charge density. We conclude from the simulations that isolated entanglements are sufficient to create molecular weight dependent bulk motion and that the probability of entanglement, as well as the duration of entanglement, is highly sensitive to all system variables. The simulations can explain some of the trends observed during capillary electrophoresis in a dilute solution of neutral polymers.

2. Model and Simulation

The Monte Carlo simulation algorithim represents the mobile probe and the frozen host as pearl-necklace chains with relative molecular weights of N and M beads, respectively. The beads, separated from attached neighbors by bonds of one Kuhn length l, define chains that are freely jointed, freely rotating, and three-dimensional. Each bead possesses a hard core diameter α large enough to prevent bond crossings during equilibration and simulated electrophoresis dynamics. Thus, monomer i and monomer j, which are separated by distance $r_{i,j}$ experience a binary hard core repulsion V_1:

$$V_1(r_{i,j}) = \begin{cases} 0 & \text{if } r_{i,j} > \alpha \\ \infty & \text{if } r_{i,j} \le \alpha \end{cases} \tag{1}$$

Note that the indices i and j extend over both chains. A percentage p of the beads comprising the probe chain are endowed with a unit negative charge, and these beads repel each other through a dimensionless Debye−Hückel potential,

$$V_2(r_{i,j}) = \beta \frac{q_i q_j}{r_{i,j}} \exp(-\kappa r_{i,j}) \tag{2}$$

where $q = -1$ or 0, and κ^{-1} is the electrostatic screening or Debye length, a parameter governed in actual experiments by the concentration of dissolved ions,

$$\kappa^2 = 4\pi\beta \sum_i c_i z_i^2 \tag{3}$$

where c_i and z_i are the concentration and valence, respectively, of the ith ion. The Bjerrum length β can be regarded as the distance over which two unscreened unit charges interact with the ambient thermal energy, i.e.,

$$\beta = \frac{e^2}{4\pi\epsilon_0\epsilon kT} \tag{4}$$

where e is the electron charge, ϵ is the solvent dielectric constant, ϵ_0 is the permittivity of vacuum, k is the Boltzmann constant, and T is the temperature. The value of β chosen for the simulations corresponds to water ($\epsilon = 78$) at 300 K.

Probe chains move through the continuous phase according to the kink−jump algorithm, with each configurational change initiated by selection of a random backbone bead m. If not at the chain end, the bead is rotated through a random angle ϕ about an axis formed by the bead's two attached neighbors. For an end bead, rotation of the terminal bond about two randomly chosen angles ϕ and θ determines the bead's new position. All movements are subjected to an excluded volume test, of the probe chain both with itself and also with the neutral host. Satisfying excluded volume constraints, configurations are sampled according to the Metropolis alogrithm,[47] which accepts or rejects new configurations based on

the energy difference ΔE_m that accompanies the proposed configurational change

$$\Delta E_m = \sum_{i<j}\sum_{j} V_2(r_{i,j})_{\text{new}} - \sum_{i<j}\sum_{j} V_2(r_{i,j})_{\text{old}} + qeE(X_{m,\text{new}} - X_{m,\text{old}}) \quad (5)$$

where the factor $X_{m,\text{new}} - X_{m,\text{old}}$ represents the bead displacement projected along the direction of the electric field E. If $\Delta E_m < 0$, acceptance of the move is immediate, but otherwise, acceptance follows the statistical criterion

$$\exp\left(-\frac{\Delta E_m}{kT}\right) \geq w \quad (6)$$

where w is a random number chosen from the interval (0,1). Whether accepted or rejected, each attempted move is counted, and N counts define a Monte Carlo (MC) time step.

The M=200 bead host chain bears no charges and is "warmed-up" or equilibrated for 40 000 MC steps before the freezing of its configuration. Probe chains, on the other hand, vary in length, with simulations conducted for $N = 25$, 30, 40, 50, 60, 70, 100, 140, or 200 and charge densities $p = 0.5$, 0.7, or 1.0. At the extremes of p (0.5 and 1.0), we examine the influence of solvent quality by equating κ^{-1} to either 1 or 10 Kuhn lengths l; at $p = 0.7$, runs are limited to $\kappa^{-1} = 1$. At the start of a simulation, the probe chain equilibrates for N^2 MC steps in the electric field's absence and again for N^2 MC steps in the field's presence. The probe's center of mass is then positioned 20 Kuhn lengths "upstream" of the host's center of mass and released. This initial separation is sufficient to preclude probe/host interaction before release. During the second equilibration step, and again after release, the dimensionless field strength,

$$\frac{qEl}{kT} = 0.1 \quad (7)$$

remains of relatively modest value. Driven by the field, the initially undistorted and unoriented probe migrates away from its upstream position and, in most cases, passes at least partially through the host; if entanglement occurs during passage, the probe strongly deforms in the field direction. Motion continues downstream in "free solution" for an additional 200 Kuhn lengths, a distance sufficient for the probe to lose all memory of the probe/host interaction and allowing recovery of the probe's undistorted average configuration in the field. For separated probe and host, a plot of the probe's projected center of mass position vs MC time yields this chain's instantaneous drift velocity U in the field direction, and the average of this velocity provides the free solution mobility by ratio with E, $\mu = U/E$. To achieve adequate statistics, between 300 and 1200 independent simulations are gathered for each initial probe/host configuration. In a small number of cases, full bead position data are gathered, enabling a visual presentation of the entire trajectory of the probe chain and its entanglement interaction with the host. It must be pointed out that these simulations are carried out without any hydrodynamic interactions between various segments. Therefore the simulation results can be used only to get some insight into the problem but not to compare directly with experimental data. On the other hand, if the concentration of neutral polymer is sufficiently high but not yet entangled (so that Rouse dynamics is valid due to fully screened hydrodynamic interaction), then the simulation results can be compared with experiments. Another limitation of the simulation algorithm used in this paper is that we cannot reliably extend our simulations to much higher field strengths than studied here (see eq 7).

3. Results and Discussion

For various combinations of p and κ^{-1}, Figure 1 displays as a function of N the average square radius of gyration $\langle r_g^2 \rangle$ of the probe chain after equilibration in the presence of the field. In all cases, $\langle r_g^2 \rangle$ rises monotonically with N as roughly a power law, and fitted power law exponents ν_{eff} suggest average probe conformations intermediate between rod (=1) and self-avoiding walk (=$^3/_5$), with ν_{eff} rising with both p and κ^{-1}. In the absence of entanglement, the imposition of the electric field only slightly deforms the otherwise isotropic probe. For more detail on the field effect on polyelectrolyte structure, the reader is referred to a previous publication.[38]

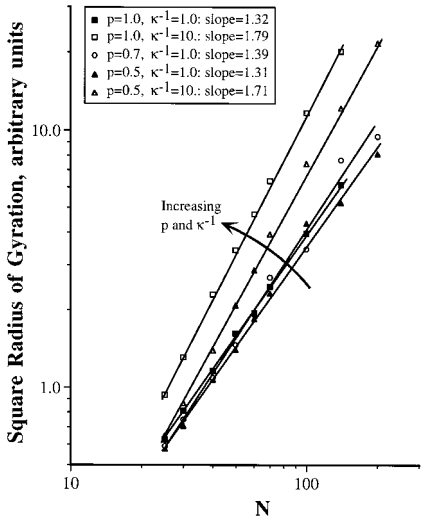

Figure 1. Mean square radius of gyration vs N.

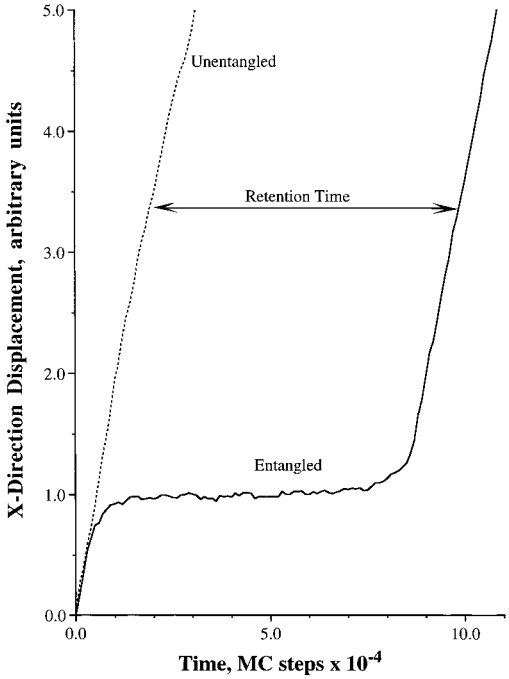

Figure 2. Typical trajectories of the field direction component of the probe center of mass vs time. ($N = 100$).

To monitor electrophoretic motion, the probe center-of-mass position is recorded at "time" intervals of 10 times N MC steps. Figure 2 illustrates center-of-mass trajectories for two simulation runs at $N = 100$. The variable x represents the projection of the center of mass of the full three-dimensional trajectories onto the field direction. In one of the plotted runs, the probe does not significantly interact with the host, and the probe's downfield velocity remains relatively constant. The

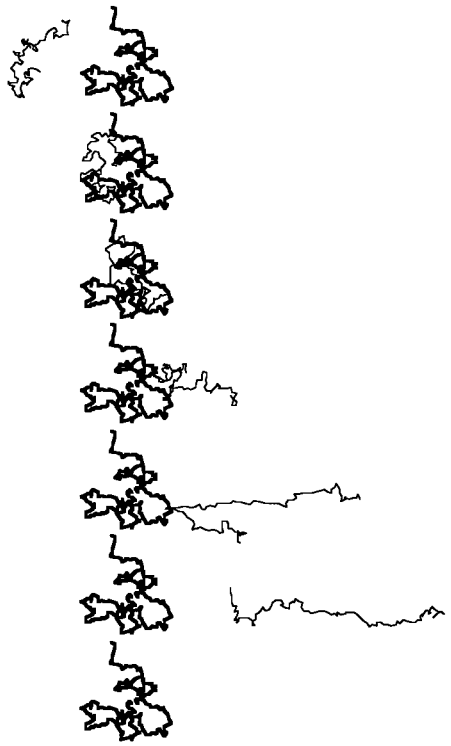

Figure 3. Typical time evolution of conformation for a probe chain in the strong entanglement case.

second trajectory, however, reveals a transient entanglement interaction that produces a substantial delay in the probe's downfield motion. In fact, during this simulation the entangled probe maintains a nearly constant center-of-mass position for a well-defined retention time t_r, measured in multiples of MC time.

Three primary modes of interaction between probe and host can be discerned within the full set of simulated chain trajectories. The first is termed a weak interaction, one in which the probe penetrates through or around the host without significant delay; a typical example is the first trajectory of Figure 2. The second mode manifests itself through an obvious delay in probe motion, but in the absence of a full fledged entanglement; these intermediate strength interactions are observed only with the longest ($N \geq 100$) probe chains. Passage of the probe through the host is achieved by a series of probe distortions, none creating a looped configuration of the probe around the host. The third and strongest interaction mode commonly evolves from the intermediate type. Here, a clear entanglement locus develops, one involving a loop of the probe chain around a single, short host segment. Figure 3 graphically illustrates a typical sequence of conformational states evolved over the course of a strong interaction, one that produces a delay of the type associated with the second trajectory of Figure 2. The most distinctive feature of Figure 3 is the abrupt appearance in the probe of a "U-shaped" hairpin turn, which subsequently disengages via a "pulley" process similar to that proposed by other authors.[45,46] During the disentanglement, the chain progresses sucessively from configurations in the U-shape to those possessing J and I shapes. The total duration of a hairpin entanglement strongly reflects the openness of the hairpin; when the arms are highly stretched and taut (as when p is large), hairpins display great persistence. Conversely, when the charge−charge repulsions are strengthened and the hairpin loosened

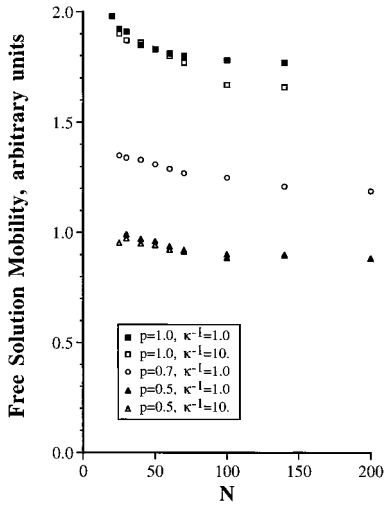

Figure 4. Dependence of free solution mobility on N and p.

(as when κ^{-1} is large), the lifetime drops. Very long chains occasionally form an "M" prior to the appearance of a "U"; in these cases, the dynamics of the "U" dominate disentanglement. Once released from the host, each probe slowly returns to its average random coil conformation as it drifts downstream. However, the sequence of undeformed−deformed−undeformed conformations is not symmetric, as the downstream relaxation occurs over much larger time and spatial scales than the initial distortion. Conformations observed in our simulation are similar to those observed by video microscopy for DNA undergoing either gel or capillary electrophoresis, as reported by the Morris group[34] and Carlsson et al.[33] Less probe distortion occurs at lower simulated field strength, but the probe also moves more slowly, making simulation runs longer and the collection of adequate statistics difficult or impossible.

The "free solution" velocity, and hence the free solution mobility μ, is obtained from the probe's post-entanglement travel, averaging 300 to 1200 data sets for each combination of probe parameters. At a fixed ratio of probe charge to probe length, the dynamics incorporated in the simulation should produce μ values dependent on p but not N, an expectation tested in Figure 4. The figure reveals a small dropoff of μ with N before the expected N independence is finally reached at $N > 100$. Actual experiments with DNA show that μ rises rather than drops to N independence.[35] The current simulation was not designed to describe these low N behaviors.

We have not substituted our simulation results into a model for the bulk mobility μ_t of a polyelectrolyte chain in dilute neutral polymer solution; one such model has recently been proposed by Slater et al.[36] We believe that μ_t can be treated as an average of two microscopic mobilities, one characterizing the entangled probe/host complex and the second characterizing the probe in free solution μ_0:

$$\mu_t = f\,\mu_e + \mu_o(1 - f) \tag{8}$$

f represents the fraction of time spent by the probe in a state of intermediate or strong interaction with the host:

$$f = \frac{t_e}{t_e + t_o} \tag{9}$$

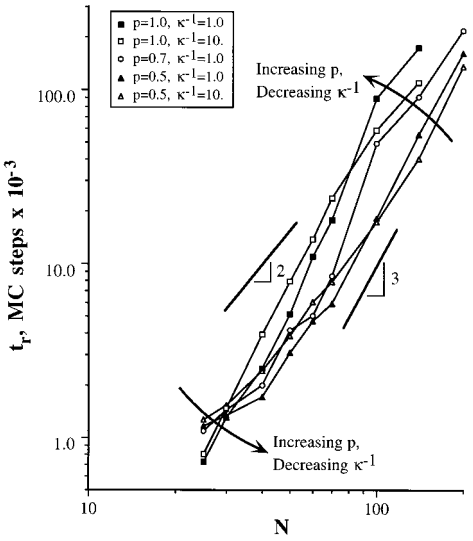

Figure 5. Dependence of retention time t_r on N, p, and κ^{-1}.

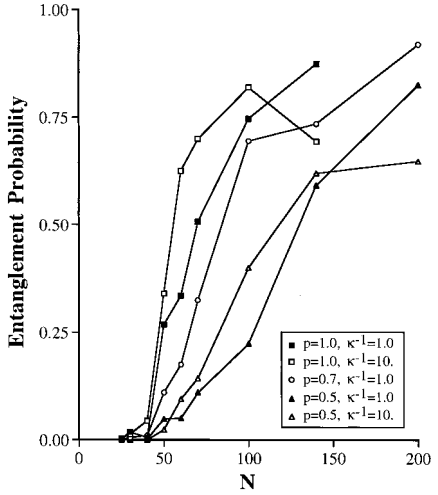

Figure 6. Probability of successful entanglement vs N.

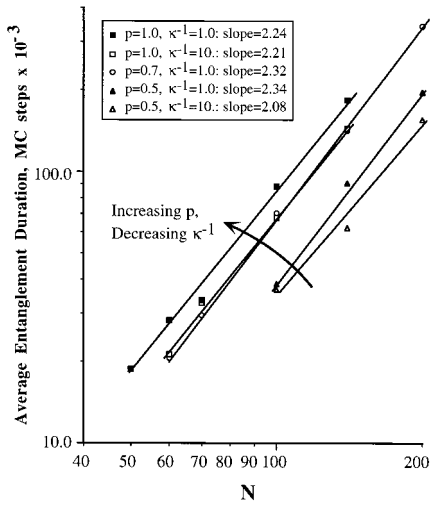

Figure 7. Average duration of successful entanglements vs N.

Although μ_0 does not depend on N, μ_t should vary with both N and M. As the host chain of the current simulation scheme is frozen in place, we limit our attention to the entanglement time t_e, i.e., the average delay in probe motion incurred by an intermediate or strong interaction. This time can be viewed as the product of the probability for entanglement (fraction of all interactions falling into the intermediate and strong category) and an average t_r of the previously defined retention time for an individual entanglement. The probability of collision depends both on the transverse diffusion coefficient of the probe and its size. Quantitative estimates of this dependence is not attempted in this paper.

To calculate t_r, probe chains for each set of run parameters are allowed to migrate until the chains reach an end position 200 Kuhn steps downstream from the host center-of-mass. Averaging of arrival times at this location defines a total transit time t_t. An unhindered transit time t_u can be calculated for the same displacement using the calculated value of μ_o. The difference, $t_t - t_u$, defines t_r.

The initial separation between probe and host was chosen to be as small as possible without the two chains overlapping. A different set of initial conditions would obviously have generated a different set of probe trajectories, and we might have hoped to calculate t_r by average over all possibile starting separations and configurational states within a large, representative solution region. Unfortunately, this immense task remains beyond the range of current simulation methods. Employing our single, "optimized" starting separation, t_r as a function of N is shown in Figure 5; each data point gathers 300 to 1200 independent simulation runs. We stress again that the averaging scheme for this plot counts all runs, including those in which the probe diffused away from the host before any possible probe−host interaction. As N becomes larger, the slope of each curve in Figure 5 approaches 3, suggesting a universal, high N regime where t_r scales roughly with N^3, when the probe and host sizes are comparable.

A more rigorous inspection of Figure 5 reveals a broad crossover near $N = 30-40$; below the crossover, chains with lower p and higher κ^{-1} display the largest values of t_r and the weakest dependence of t_r on N. Above the crossover, the first of these trends is reversed and the scaling of t_r on N becomes relatively insensitive to p and κ^{-1}. Explanation of the crossover lies in the influence of p and κ^{-1} on the entanglement process. Expanded conformations increase t_r by increasing the probability for intermediate or strong interaction; this effect extends to both short and long chains, but the relative impact for short chains is greater. Assuming that such an interaction occurs, the loosening of the hairpin entanglement at low p and high κ^{-1} makes subsequent probe disengagement more rapid, reducing t_r. At large enough N, the probability of intermediate or strong interaction approaches unity, so the dominant influence of p and κ^{-1} on t_r is felt through the disentanglement process; at low N, the dominant influence lies in their impact on the interaction probability. To differentiate more clearly between entanglement probability and entanglement persistence, we plot the probability of successful entanglement vs N in Figure 6 and the average duration of successful entanglement vs N in Figure 7. Unlike Figure 5, which encompasses the full set of simulated probe−host interactions, the two new plots are based on apportionment of the interactions into categories of successful entanglement (intermediate and strong interaction) and unsuccessful entanglement (all else). Precise distinction between the two categories can be difficult, as fluctuations in the free solution velocity are often large, especially at small p and N. Many observed

fluctuations could easily be miscategorized as successful entanglement. To minimize such sorting errors, a successful entanglement is defined conservatively, by a transit time that exceeds t_u by more than 30%. This substantial percentage ensures that only successful entanglements have been considered in the analyses leading to Figures 6 and 7, albeit with some successful entanglements disregarded. Figure 6 demonstrates that for each set of run conditions there is a narrow window of N over which the entanglement probability rises from zero to near unity. A closer examination of the individual curves, and a comparison to Figure 1, reveals that the window corresponds to approximately equal probe and host radii of gyration. The spread of curves in Figure 6 suggests that an electrophoretic separation might be tuned or optimized by controlled variation of p and/or κ^{-1}. The kinetics of probe−host entanglement are probably best manifested in Figure 7, which demonstrates a power law dependence of average entanglement duration on N for all run conditions. Pulley-like unraveling of hairpin-distorted probe chains dominates the entanglement process, and as previously mentioned, this unraveling is accelerated at small p and large κ^{-1}. The power law exponent that best fits these curves appears to be almost universal, varying between 2.08 and 2.34. For release of entanglement by Rouse-dominated diffusion, the exponent would be 2.0, while for release by reptation-dominated diffusion, the exponent would be 3.0. Although our exponent is nearer to 2.0 than 3.0, direct visualizations such as Figure 3 convincingly demonstrate that simple Rouse dynamics are not responsible for probe disengagement. In fact, the unraveling chain undergoes an evolution in structure more consistent with reptation. Because of the finite applied field, reptation refers to the biased reptation model developed by Lumpkin, Dejardin, and Zimm[21] and Slater and Noolandi.[25−27] Nevertheless, the weaker N dependence observed in the current simulations must result from the significant configurational fluctuations permitted at the chosen field strength, and these fluctuations appear sufficient to regulate the disentanglement process.

4. Conclusions

The interaction of a mobile polyelectrolyte chain and a single neutral host can endow the polyelectrolyte with a strongly molecular weight dependent mobility, even in absence of host mobility. The dominant interaction can be characterized as a U-shaped probe entanglement with the host. Despite the distorted nature of the entanglement and its release by unraveling, the kinetics remain dominated by Brownian fluctuations in the probe's configuration. Using the discrete kinetics uncovered by the simulation, we believe that the construction of a more accurate bulk model for capillary electrophoresis in a dilute solution of neutral polymers will be possible.

In addition to the development of this model, several specified questions remain in regards to discrete probe−host interactions in an electric field. Future work will address both the influence of host mobility on the interaction and the variation in response as the constant field magnitude is altered. Use of multiple hosts and variation of host−probe size ratio may answer practical questions pertaining to the selection of optimal host molecular weight and concentration. Although hydrodynamic interaction is absent in the present Monte Carlo simulations, the role of multiple host chains in determining the mobility of the probe will be addressed in the future with the hope that more insight might be gained and that hydrodynamics might be sufficiently screened at higher concentrations of the neutral chains. Most of all, given the numerical difficulty of realistic simulations, we see a need for careful experimental measurements to elucidate more clearly how the numerous operational variables affect separation.

Acknowledgment. Financial support from the Materials Research Science and Engineering Center at the University of Massachusetts is gratefully acknowledged. The authors thank D. Srivastava for help during th initial stages of the programming.

References and Notes

(1) Barron, A. E.; Sunada, W. M.; Blanch, H. W. *Biotechnol. Bioeng.* **1996**, *52*, 259.
(2) Barron, A. E.; Soane, D. S.; Blanch, H. W. *J. Chromatogr.* **1993**, *652*, 3.
(3) Barron, A. E.; Blanch, H. W.; Soane, D. S. *Electrophoresis* **1994**, *15*, 597.
(4) Schwinefus, J. J.; Wang, S.-C.; Hammond, R. W.; Morris, M. D. *Electrophoresis* **1996**, *17*, 1110.
(5) Olvera, B. M.; Baine, P.; Davidson, N. *Biopolymers* **1964**, *2*, 245.
(6) Zimm, B. H.; Levene, S. D. *Q. Rev. Biophys.* **1992**, *25* (2), 171.
(7) Hieger, D. N.; Cohen, A. S.; Karger, B. L. *J. Chromatogr.* **1990**, *516*, 33.
(8) D. Tietz, D.; Gottlieb, M. H.; Fawcett, J. S.; Chrambach, A. *Electrophoresis* **1986**, *7*, 217.
(9) Strege, M.; Lagu, A. *Anal. Chem.* **1991**, *63*, 1233.
(10) Nakatani, M.; Shibukawa, A.; Nakagawa, T. *J. Chromatogr. A* **1994**, *672*, 213.
(11) Baba, Y.; Ishimaru, N.; Samata, K.; Tsuhaku, M. *J. Chromatogr.* **1993**, *653*, 329.
(12) Izumi, T.; Yamaguchi, M.; Yonenda, K.; Isobe, T.; Okuyama, T.; Shinoda, T. *J. Chromatogr.* **1993**, *652*, 41.
(13) Bocek, P.; and Chrambach, A. *Electrophoresis* **1991**, *12*, 1059.
(14) Chang, H.-T.; Yeung, E. S. *J. Chromatogr. B* **1995**, *669*, 113.
(15) Grossman, P. D.; Soane, D. S. *J. Chromatogr.* **1991**, *559*, 257.
(16) Ogsten, A. G. *Trans. Faraday Soc.* **1958**, *54*, 1754.
(17) Rodbard, D.; Chrambach, A. *Proc. Nat. Acad. Sci. U.S.A.* **1970**, *65*, 970.
(18) Arvanitidou, E.; Hoagland, D. A.; Smisek, D. *Biopolymers* **1991**, *31*, 435.
(19) Slater, G.W.; Guo, H. L. *Electrophorsis* **1996**, *17*, 977.
(20) De Gennes, P. G. *J. Chem. Phys.* **1972**, *55*, 572.
(21) Lumpkin, O. J.; Dejardin, P.; Zimm, B. H. *Biopolymers* **1985**, *24*, 1573.
(22) Duke, T. A. J.; Semenov, A. N.; Viovy, J. L. *Phys. Rev. Lett.* **1992**, *69*, 3260.
(23) Semenov, A. N.; Duke, T. A.; Viovy, J. L. *Phys. Rev. E* **1995**, *51*, 1520.
(24) Slater, G. W.; Noolandi, J. *Biopolymers* **1986**, *25*, 431.
(25) Slater, G. W.; Noolandi, J. *Biopolymers* **1985**, *24*, 2181.
(26) Slater, G. W.; Rousseau, J.; Noolandi, J. *Biopolymers* **1987**, *26*, 863.
(27) Slater, G. W.; Noolandi, J. *Biopolymers* **1989**, *28*, 1781.
(28) Muthukumar, M.; Baumgärtner, A. *Macromolecules* **1989**, *22*, 1937.
(29) Muthukumar, M. *J. Noncryst. Solids* **1991**, *131−133*, 654.
(30) Hoagland, D. A.; Muthukumar, M. *Macromolecules* **1992**, *25*, 6696.
(31) Rousseau, J.; Drouin, G.; Slater, G. W. *Phys. Rev. Lett.* **1997**, *79*, 1945.
(32) Singhal, R. P.; Xian, J. *J. Chromatogr. A* **1993**, *652*, 47.
(33) Carlsson, C.; Larsson, M.; Jonsson, M.; Norden, B. *J. Am. Chem. Soc.* **1995**, *117*, 3871.
(34) Shi, X.; Hammond, R. W.; Morris, M. D. *Anal. Chem.* **1995**, *67*, 1132.
(35) Völkel, A. R.; Noolandi, J. *Macromolecules* **1995**, *28*, 8182.
(36) Hubert, H. J.; Slater, G. W.; Viovy, J. L. *Macromolecules* **1996**, *29*, 1006.
(37) Muthukumar, M. *Electrophoresis* **1996**, *17*, 1167.

(38) Melenkevitz, J.; Muthukumar, M. *Chemtracts—Macromol. Chem.* **1990**, *1*, 171.
(39) Deutch, J. M.; Madden, T. L. *J. Chem. Phys.* **1989**, *90*, 2476.
(40) Shaffer, E. O.; Olvera de la Cruz, M. *Macromolecules* **1989**, *22*, 1351.
(41) Duke, T. A. J. *J. Chem. Phys.* **1990**, *93*, 9049.
(42) Batoulis, J.; Pistoor, N.; Kremer, K.; Frisch, H. L. *Electrophoresis* **1989**, *10*, 442.
(43) Volkmuth, W. D.; Duke, T.; Wu, M. C.; Austin, R. H.; Szabo, A. *Phys. Rev. Lett.* **1994**, *72*, 2117.
(44) Noolandi, J.; Rousseau, J.; Slater, G.W.; Turmel, C.; Lalande, M. *Phys. Rev. Lett.* **1987**, *58*, 2428.
(45) Sevick, E. M.; Williams, D. R. M. *Phys. Rev. Lett.* **1996**, *76*, 2595.
(46) Nixon, G. I.; and Slater, G. W. *Phys. Rev. E* **1994**, *50*, 5033.
(47) Metropolis, N.; Rosenbluth, A. W.; Rosenbluth, A. W.; Teller, A. H.; and Teller, E. J. *J. Chem. Phys.* **1953**, *21*, 1098.

MA971651R